

Ab initio calculation of hyper-neutron matter

Hui Tong,¹ Serdar Elhatisari,^{2,3,1} and Ulf-G. Meißner^{1,4,5,6,7}

¹Helmholtz-Institut für Strahlen- und Kernphysik and Bethe Center for Theoretical Physics, Universität Bonn, D-53115 Bonn, Germany

²Faculty of Natural Sciences and Engineering, Gaziantep Islam Science and Technology University, Gaziantep 27010, Turkey

³Interdisciplinary Research Center for Industrial Nuclear Energy (IRC-INE),

King Fahd University of Petroleum and Minerals (KFUPM), 31261 Dhahran, Saudi Arabia

⁴Institute for Advanced Simulation (IAS-4), Forschungszentrum Jülich, D-52425 Jülich, Germany

⁵Center for Advanced Simulation and Analytics (CASA), Forschungszentrum Jülich, D-52425 Jülich, Germany

⁶Tbilisi State University, 0186 Tbilisi, Georgia

⁷Peng Huanwu Collaborative Center for Research and Education, Beihang University, Beijing 100191, China

(Dated: February 24, 2025)

In the era of multi-messenger astronomy, neutron stars arguably stand out as the most captivating astrophysical objects [1]. Neutron stars consist of the densest form of baryonic matter observed in the universe, and within their interiors, exotic new forms of matter may exist [2]. With the detection of various neutron star phenomena in recent years, such as gravitational waves and electromagnetic radiation, more valuable information regarding the mysterious dense matter within their cores will be unraveled. These findings, together with the measurements of the masses or radii, strongly constrain the neutron star matter equation of state (EoS) and theoretical models of their composition. However, the observation of neutron star masses above $2.0M_{\odot}$ has ruled out many predictions of exotic non-nucleonic components. Resolving this problem, known as the hyperon puzzle, is crucial for understanding the complex interplay between strong nuclear forces and the behavior of dense matter under extreme conditions [3, 4].

In this study, we use the framework of Nuclear Lattice Effective Field Theory (NLEFT) [5] to gain new insights into the generation of hyperons, more specifically $\Lambda(1116)$ particles, within dense environments. To enable calculations with arbitrary numbers of nucleons and hyperons using only one auxiliary field, we introduce a novel formulation of the auxiliary field quantum Monte Carlo (AFQMC) algorithm, which allows for more accurate and efficient simulations free of sign oscillations. Additionally, we incorporate two-body $N\Lambda$ and $\Lambda\Lambda$ interactions, as well as three-body terms such as $NN\Lambda$ and $N\Lambda\Lambda$, based on the minimal nuclear interaction model [6], into the pionless effective field theory for nucleons. Initially, we focus on systems consisting solely of nucleons and determine the low-energy constants parameterizing the $2N$ and the $3N$ forces by constraining them to the saturation properties of symmetric nuclear matter, as it is well-known that fixing the $3N$ forces in light nuclei leads to a serious overbinding in heavier systems [7] if mostly local forces are employed. After constructing our interactions, we perform predictive calculations for the EoS of pure neutron matter (PNM) by considering up to 232 neutrons in a box to achieve densities up to five times the empirical saturation density of nuclear matter, i.e., $\rho = 0.8 \text{ fm}^{-3}$. Our results for the EoS of PNM are in very good agreement with *ab initio* calculations using chiral interactions up to N3LO [7] within the

given density range. Subsequently, we introduce Λ -particles into our framework and determine the parameters of the $N\Lambda$ and $\Lambda\Lambda$ interactions by fitting them to experimental data, including the $N\Lambda$ cross section [8] and the $\Lambda\Lambda$ 1S_0 scattering phase shift from chiral effective field theory [9], respectively. The $NN\Lambda$ and $N\Lambda\Lambda$ forces are further constrained by the separation energies of single- and double- Λ hypernuclei, spanning systems from $^5_{\Lambda}\text{He}$ to $^6_{\Lambda\Lambda}\text{Be}$, denoted as HNM(I). It is difficult to probe the behavior of the EoS at high densities encountered in neutron stars in terrestrial laboratories, and various phenomenological schemes [10] and microscopical models [3] suggest that hyperons emerge in the inner core of neutron stars at densities around $\rho \approx (2 - 3)\rho_0$. Therefore, similar to using the saturation properties of symmetric nuclear matter to pin down the three-nucleon forces (3NFs), we alternatively determined the $NN\Lambda$ and $N\Lambda\Lambda$ forces by using the separation energies of hypernuclei and the Λ threshold densities $\rho_{\Lambda}^{\text{th}}$ around $(2 - 3)\rho_0$ simultaneously in HNM(II) and HNM(III). We set $\rho_{\Lambda}^{\text{th}} = 0.398(2)(5)$ and $0.520(2)(6) \text{ fm}^{-3}$ for HNM(II) and HNM(III), respectively. In the next step, we perform simulations for hyper-neutron matter by including up to 116 hyperons in the box and calculate the corresponding EoSs. More details on the construction of the actions underlying PNM EoS and the three variants of HNM are given in the Supplementary materials.

The results for pure neutron matter and hyper-neutron matter are presented from our state-of-art nuclear lattice simulations. HNM is composed of neutrons and Λ hyperons, where ρ_N , ρ_{Λ} , and $\rho = \rho_N + \rho_{\Lambda}$ are the neutron, Λ hyperon and total baryon density of the system, respectively, and $x_{\Lambda} = \rho_{\Lambda}/\rho$ is the fraction of Λ hyperons. The Λ threshold densities $\rho_{\Lambda}^{\text{th}}$ is determined by imposing the equilibrium condition $\mu_N = \mu_{\Lambda}$, where the chemical potentials for neutrons μ_N and lambdas μ_{Λ} are evaluated via the derivatives of the energy density ε_{HNM} ,

$$\mu_N(\rho, x_{\Lambda}) = \frac{\partial \varepsilon_{\text{HNM}}}{\partial \rho_N}, \quad \mu_{\Lambda}(\rho, x_{\Lambda}) = \frac{\partial \varepsilon_{\text{HNM}}}{\partial \rho_{\Lambda}}, \quad (1)$$

which indicates that an accurate determination of the chemical potentials necessitates computing the energy density for various densities and different numbers of Λ hyperons.

In Fig. 1, the EoSs for PNM and for HNM are displayed. As anticipated, the inclusion of hyperons results in a softer

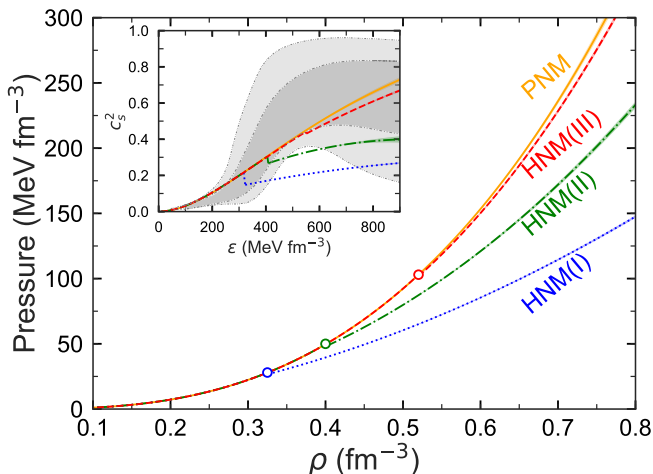


FIG. 1. (Color online) EoS for HNM. The orange solid curve denotes pure neutron matter, obtained from the NN and NNN interactions. The red dashed line represents the EoS of HNM with hyperons interacting via the two-body interactions ($N\Lambda$ and $\Lambda\Lambda$) and the third set of three-body hyperon-nucleon interaction ($NN\Lambda$ and $N\Lambda\Lambda$). The blue dotted curve and the green dot-dashed curve are calculated with the first and second sets of three-body hyperon-nucleon interactions. The Λ threshold densities $\rho_{\Lambda}^{\text{th}}$ are marked by open circles. In the inset, the speed of sound corresponding to the PNM and HNM EOSs is shown. The gray shaded regions are the inference of the speed of sound for neutron star matter in view of the recent observational data [11].

EoS, and the threshold density is $\rho_{\Lambda}^{\text{th}} = 0.325(2)(4) \text{ fm}^{-3}$ for HNM(I). Here and what follows, the first (second) error is the statistical (systematic) one. This threshold aligns with predictions from various phenomenological schemes [10] and microscopical models [3], which suggest that hyperons emerge in the inner core of neutron stars at densities around $\rho \approx (2 - 3)\rho_0$. Furthermore, we construct two additional variants of HNM, denoted as HNM(II) and HNM(III). The EoS becomes stiffer at higher densities for these variants, indicating the inclusion of more repulsion in the three-body hyperon-nucleon interactions. The squared speed of sound, c_s^2 , is also shown in the inset of Fig. 1. It is observed that the causality limit ($c_s^2 < 1$) is fulfilled for both PNM and HNM. It should be noted that in the pioneering calculations of Lonardonì et al. [4], they performed auxiliary field diffusion Monte Carlo (AFDMC) simulations with $N_n = 38, 54, 66$ neutrons and their PNM EoS is stiffer than ours and exceeds the causality limit for the speed of sound at densities above $\rho \simeq 0.68 \text{ fm}^{-3}$. The EoS characterized by nucleonic degrees of freedom exclusively demonstrate a monotonic increase in c_s^2 with increasing energy density. The appearances of Λ hyperons, however, induces changes in this behavior, leading to non-monotonic curves that signify the incorporation of additional degrees of freedom. The onset of Λ hyperons precipitates a sharp reduction in the speed of sound, marking a significant transition in the stiffness of the EoS. For comparison, the constraints on c_s^2 within the interiors of neutron stars inferred by a Bayesian

inference method are also shown [11]. These constraints are established based on recent multi-messenger data, in combination with limiting conditions from nuclear physics at low densities, as depicted by the gray shaded regions. The results for PNM and HNM(III) agree well with the marginal posterior probability distributions at the 95% and 68% levels. It should be noted that we used the minimal nuclear interaction field theory [7]. In Ref. [7], a full chiral interactions at next-to-next-to-next-to-leading order (N³LO) was used for PNM and symmetric nuclear matter. This significantly increases the computational cost so that the calculations were done only at densities up to $2\rho_0$. In the future, we will incorporate the methodological advancements introduced in this work to explore neutron star EoS calculations using higher order chiral forces at densities larger than $2\rho_0$. While our calculations extend into the higher-density regime, we recognize that the behavior of EoS at these densities is less constrained, and the nuclear interaction models we employ may introduce uncertainties. To validate the nuclear interaction model in this work, we have quantified the theoretical uncertainty due to the six different three-nucleon forces which are shown in Fig. 1 and Fig. S2. We find the theoretical uncertainty in Fig. S2 is significantly smaller than the empirical uncertainty of the nuclear matter, and the uncertainty is also quite small for PNM in Fig. 1. This uncertainty quantification provides a solid foundation for future research on uncertainties in hyper-neutron matter, as the hyperonic three-baryon interactions used in our calculations follow the same uncertainty quantification approach. Therefore, the uncertainty in our nuclear interaction models has been significantly reduced and is well controlled. Due to the current limitations of computational resources, calculating the EoS for arbitrary fractions of protons, neutrons, and other hyperons is still very challenging in any lattice approach. This can be achieved when more computational resources become available in the future and it will allow us to avoid the errors introduced by using the so-called symmetry energy approximation.

The ‘‘holy grail’’ of neutron-star structure, the mass-radius (MR) relation, is displayed in Fig. 2. These relations for PNM and HNM are obtained by solving the Tolman-Oppenheimer-Volkoff (TOV) equations with the EoSs of Fig. 2. The appearance of Λ hyperons in neutron star matter remarkably reduces the predicted maximum mass compared to the PNM scenario. The maximum mass for PNM, HNM(I), HNM(II), and HNM(III) are $2.19(1)(1) M_{\odot}$, $1.59(1)(1) M_{\odot}$, $1.94(1)(1) M_{\odot}$, and $2.17(1)(1) M_{\odot}$, respectively. Three neutron stars have been measured to have gravitational masses close to $2M_{\odot}$: PSR J1614-2230, with $M = 1.908 \pm 0.016 M_{\odot}$ [15]; PSR J0348+0432, with $2.01 \pm 0.04 M_{\odot}$ [16]; and PSR J0740+6620, with $2.08 \pm 0.07 M_{\odot}$ [17]. These measurements significantly constrain the EoS of dense nuclear matter, ruling out the majority of currently proposed EoSs with hyperons from phenomenological approaches [18]. Our results show that the inclusion of the $N\Lambda$ and $N\Lambda\Lambda$ interaction in HNM(III) leads to an EoS stiff enough such

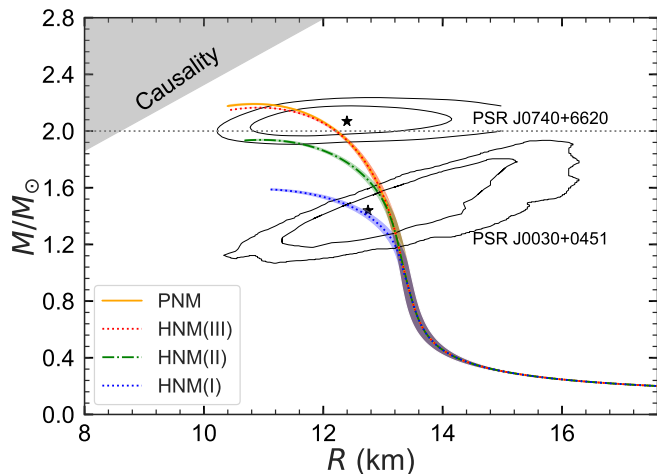


FIG. 2. (Color online) Neutron star mass-radius relation. The legend is the same as of Fig. 1. The gray horizontal dotted line represents $2M_{\odot}$. The inner and outer contours indicate the allowed area of mass and radius of neutron stars by NICER’s analysis of PSR J0030+0451 [12] and PSR J0740+6620 [13]. The excluded causality region is also shown by the grey shaded region [14].

that the resulting neutron star maximum mass is compatible with the three mentioned measurements of neutron star masses. Therefore, the repulsion introduced by the hyperonic three-body interactions plays a crucial role, since it substantially increases the value of the Λ threshold density. It is also noteworthy that HNM(I) predicts a maximum mass above the canonical neutron mass of $1.4M_{\odot}$, whereas the model (I) incorporating repulsive $NN\Lambda$ interactions in the auxiliary field diffusion Monte Carlo [4], Hartree-Fock [19], and Brueckner-Hartree-Fock (BHF) [3, 20] calculations yield values below $1.4M_{\odot}$. In addition, the radii corresponding to PNM, HNM(I), HNM(II), and HNM(III) are $R_{1.4M_{\odot}} = 13.10(1)(7)$ km, $R_{1.4M_{\odot}} = 12.71(4)(13)$ km, $R_{1.4M_{\odot}} = 13.09(1)(8)$ km, and $R_{1.4M_{\odot}} = 13.10(1)(7)$ km, in order. Our results for the neutron star radii are also consistent with the constraints by NICER [12] for the mass and radius of PSR J0030+0451, i.e., mass $1.44^{+0.15}_{-0.14}M_{\odot}$ with radius $13.02^{+1.24}_{-1.06}$ km. The 68% and 95% contours of the joint probability density distribution of the mass and radius from the NICER analysis are also shown in Fig. 2. We further note that despite the significant reduction in the fraction of Λ hyperons caused by the hyperonic three-body force in HNM(III), they still exist within the interior of a $2.17M_{\odot}$ neutron star. This is different from the conclusion drawn in Ref. [4], where it was found the hyperonic three-body force in their parametrization (II) capable of generating an EoS stiff enough to support maximum masses consistent with the observations of $2M_{\odot}$ neutron stars results in the complete absence of Λ hyperons in the cores of these objects. We also note that while model HNM(III) successfully supports the mass of PSR J0740+6620 with $2.08 \pm 0.07 M_{\odot}$, the $M(R)$ curve appears only marginally compatible with the combined experimental data. This issue is primarily associated with two fac-

tors. First, the characteristics of this neutron star mass region are predominantly determined by the EoS at higher densities. The baryon-baryon interactions considered in this work account only for contributions from the minimal interaction model, whereas higher-order baryon-baryon interactions are expected to influence the EoS at higher densities. Therefore, it will be interesting and necessary to include the higher-order baryon-baryon interactions in the subsequent work. Second, the rotation of a neutron star induces corresponding increases in both its mass and radius, which can lead to a better agreement with the combined experimental data. The rotational frequency of this neutron star is 346 Hz, while the current calculations have been limited to static case. In the next step, we will incorporate the properties of rotating neutron stars.

In summary, we have performed the first lattice Monte Carlo calculation of hyper-neutron matter with a large number of neutrons and Λ s and derived the resulting properties of neutron stars. In the next steps, one should include the proton fraction, other hyperons of the baryon octet, and make use of the recently developed high-fidelity chiral interactions at N3LO [7], though this will pose a formidable computational challenge.

Conflict of interest

The authors declare that they have no conflict of interest.

Acknowledgments

We are grateful for discussions with members and partners of the Nuclear Lattice Effective Field Theory Collaboration, in particular Zhengxue Ren. We are deeply thankful to Wolfram Weise for some thoughtful comments. Hui Tong thanks Jie Meng and Sibao Wang for helpful discussions. Serdar Elhatisari thanks Dean Lee for useful discussions on the auxiliary field formulations. We acknowledge funding by the European Research Council (ERC) under the European Union’s Horizon 2020 research and innovation programme (AdG EXOTIC, grant agreement No. 101018170), by the MKW NRW under the funding code NW21-024-A and by DFG and NSFC through funds provided to the Sino-German CRC 110 “Symmetries and the Emergence of Structure in QCD” (NSFC Grant No. 12070131001, DFG Project-ID 196253076). The work of Serdar Elhatisari was further supported by the Scientific and Technological Research Council of Turkey (TUBITAK project no. 120F341). The work of Ulf-G. Meißner was further supported by CAS through the President’s International Fellowship Initiative (PIFI) (Grant No. 2025PD0022).

Author contributions

The project was initiated and supervised by Ulf-G. Meißner. Serdar Elhatisari conceived the AFMC formulation for hypernuclear system, and code development, testing and optimization were led by Serdar Elhatisari with contributions by Hui Tong. Hui Tong performed the analysis of the data with contributions by Serdar Elhatisari, led production runs, and created the figures. All authors contributed to the writing.

-
- [1] Abbott BP, Abbott R, Abbott TD, et al. GW170817: Observation of gravitational waves from a binary neutron star inspiral. *Phys Rev Lett* 2017;119:161101
 - [2] Lattimer JM, Prakash M. The physics of neutron stars. *Science* 2004;304:536-542
 - [3] Schulze HJ, Rijken T. Maximum mass of hyperon stars with the nijmegen es c-08 model. *Phys Rev C* 2011;84:035801
 - [4] Lonardoni D, Lovato A, Gandolfi S, et al. Hyperon puzzle: hints from quantum monte carlo calculations. *Phys Rev Lett* 2015;114:092301
 - [5] Lähde TA, Meißner UG. Nuclear lattice effective field theory: an introduction. Heidelberg: Springer 2019;957
 - [6] Lu BN, Li N, Elhatisari S, et al. Essential elements for nuclear binding. *Phys Lett B* 2019;797:134863
 - [7] Elhatisari S, Bovermann L, Ma YZ, et al. Wavefunction matching for solving quantum many-body problems. *Nature* 2024;630:59-63
 - [8] Sechi-Zorn B, Kehoe B, Twitty J, et al. Low-energy lambda-proton elastic scattering. *Phys Rev* 1968;175:1735-1740
 - [9] Haidenbauer J, Meißner UG, Petschauer S. Strangeness $S = -2$ baryon-baryon interaction at next-to-leading order in chiral effective field theory. *Nucl Phys A* 2016;954:273-293
 - [10] Weber F, Weigel MK. Baryon composition and macroscopic properties of neutron stars. *Nucl Phys A* 1989;505:779-822
 - [11] Brandes L, Weise W, Kaiser N. Evidence against a strong first-order phase transition in neutron star cores: impact of new data. *Phys Rev D* 2023;108:094014
 - [12] Müller MC, Lamb FK, Dittmann AJ, et al. PSR J0030+0451 mass and radius from *NICER* data and implications for the properties of neutron star matter. *Astrophys J Lett* 2019;887:L24
 - [13] Riley TE, Watts AL, Ray PS, et al. A *NICER* view of the massive pulsar PSR J0740+6620 informed by radio timing and *XMM-newton* spectroscopy. *Astrophys J Lett* 2021;918:L27
 - [14] Lattimer JM, Prakash M. Neutron star observations: prognosis for equation of state constraints. *Phys Rept* 2007;442:109-165
 - [15] Demorest P, Pennucci T, Ransom S, et al. Shapiro delay measurement of a two solar mass neutron star. *Nature* 2010;467:1081-1083
 - [16] Antoniadis J, Freire PCC, Wex N. A massive pulsar in a compact relativistic binary. *Science* 2013;340:6131
 - [17] Fonseca E, Cromartie HT, Pennucci TT, et al. Refined mass and geometric measurements of the high-mass PSR J0740+6620. *Astrophys J Lett* 2021;915:L12
 - [18] Burgio GF, Schulze HJ, Vidana I, et al. Neutron stars and the nuclear equation of state. *Prog Part Nucl Phys* 2021;120:103879
 - [19] Dapo H, Schaefer, BJ, Wambach J. On the appearance of hyperons in neutron stars. *Phys Rev C* 2010;81:035803
 - [20] Wang SB, Tong H, Wang CC, et al. Tensor-force effects on nuclear matter in relativistic ab initio theory. *Sci Bull* 2024;69:2166-2169

SUPPLEMENTAL MATERIALS

Nuclear Lattice Effective Field Theory

Lattice Formalism

Lattice effective field theory is a quantum many-body method that synthesises the theoretical framework of effective field theory (EFT) with powerful numerical approaches [1, 2]. The method has been applied to describe the properties of atomic nuclei [3] and neutron matter [4] in pionless EFT at leading order (LO), and to perform the first *ab initio* calculation of the Hoyle state in the spectrum of ^{12}C [5] and α - α scattering [6] in chiral EFT at next-to-next-to-leading order (N2LO). Moreover, it has recently been applied to compute the properties of atomic nuclei and the equation of state of neutron and symmetric nuclear matter in chiral EFT at next-to-next-to-next-to-leading order (N3LO) [7]. In addition, the method has been used in formulating an EFT with only four parameters and built on Wigner's SU(4) spin-isospin symmetry [8]. This EFT effectively captures gross properties of light and medium-mass nuclei and the equation of state of neutron matter with remarkable accuracy, typically within a few percent [9]. Noteworthy applications of this EFT include the study of the first *ab initio* thermodynamics calculation of nuclear clustering [10] and microscopic investigations of clusters in hot dilute matter using the method of light-cluster distillation [11], and the identification of the emergent geometry and intrinsic cluster structure of the low-lying states of ^{12}C [12, 13]. Additionally, it has been utilized in resolving the puzzle of the alpha-particle monopole transition form factor [14].

Building upon the significant achievements of the EFT within Wigner's SU(4) spin-isospin symmetry, which we refer to as the minimal nuclear interaction, throughout this paper we exclusively define and employ pionless EFT at LO for nucleons (see also [15]), derived from this minimal nuclear interaction. This approach allows us to make use of the well-established theoretical framework by the minimal nuclear interaction, providing a solid basis for our calculations for hyper-neutron matter equations of state. It is important to note that our calculations consider only Λ hyperons, with the inclusion of Σ hyperons reserved for future work. Note that the Λ - Σ^0 transition induces three-body forces which are effectively represented by ΛNN forces here.

For the hyperon-nucleon and hyperon-hyperon interactions, we also utilize minimal interactions assuming that these interactions are spin symmetric. Therefore, the Hamiltonian is defined as,

$$\begin{aligned}
 H = & H_{\text{free}} + \frac{c_{NN}}{2} \sum_{\vec{n}} : [\tilde{\rho}(\vec{n})]^2 : + \frac{c_{NN}^T}{2} \sum_{I, \vec{n}} : [\tilde{\rho}_I(\vec{n})]^2 : \\
 & + c_{N\Lambda} \sum_{\vec{n}} : \tilde{\rho}(\vec{n}) \tilde{\xi}(\vec{n}) : + \frac{c_{\Lambda\Lambda}}{2} \sum_{\vec{n}} : [\tilde{\xi}(\vec{n})]^2 : \\
 & + V_{NN}^{\text{GIR}} + V_{N\Lambda}^{\text{GIR}} + V_{\Lambda\Lambda}^{\text{GIR}} + V_{\text{Coulomb}} \\
 & + V_{NNN} + V_{NN\Lambda} + V_{N\Lambda\Lambda}, \tag{S1}
 \end{aligned}$$

where H_{free} is the kinetic energy term defined by using fast Fourier transforms to produce the exact dispersion relations $E_N = p^2/(2m_N)$ and $E_\Lambda = p^2/(2m_\Lambda)$ with nucleon mass $m_N = 938.92$ MeV and hyperon mass $m_\Lambda = 1115.68$ MeV, the $::$ symbol indicates normal ordering, c_{NN} is the coupling constant of the SU(4) symmetric short-range two-nucleon interaction, c_{NN}^T is the coupling constant of the isospin-dependent short-range two-nucleon interaction, that breaks SU(4) symmetry (see the discussion below), $c_{N\Lambda}$ ($c_{\Lambda\Lambda}$) is the coupling constant of the spin-symmetric short-ranged hyperon-nucleon (hyperon-hyperon) interaction, and $\tilde{\rho}$ ($\tilde{\xi}$) is nucleon (hyperon) density operator, that is smeared both locally and non-locally,

$$\tilde{\rho}(\vec{n}) = \sum_{i,j=0,1} \tilde{a}_{i,j}^\dagger(\vec{n}) \tilde{a}_{i,j}(\vec{n}) + s_L \sum_{|\vec{n}-\vec{n}'|=1} \sum_{i,j=0,1} \tilde{a}_{i,j}^\dagger(\vec{n}') \tilde{a}_{i,j}(\vec{n}'), \tag{S2}$$

$$\tilde{\rho}_I(\vec{n}) = \sum_{i,j,j'=0,1} \tilde{a}_{i,j}^\dagger(\vec{n}) [\tau_I]_{j,j'} \tilde{a}_{i,j'}(\vec{n}) + s_L \sum_{|\vec{n}-\vec{n}'|=1} \sum_{i,j,j'=0,1} \tilde{a}_{i,j}^\dagger(\vec{n}') [\tau_I]_{j,j'} \tilde{a}_{i,j'}(\vec{n}'), \tag{S3}$$

$$\tilde{\xi}(\vec{n}) = \sum_{i=0,1} \tilde{b}_i^\dagger(\vec{n}) \tilde{b}_i(\vec{n}) + s_L \sum_{|\vec{n}-\vec{n}'|=1} \sum_{i=0,1} \tilde{b}_i^\dagger(\vec{n}') \tilde{b}_i(\vec{n}'). \tag{S4}$$

The smeared annihilation and creation operators, \tilde{a} (\tilde{b}) and \tilde{a}^\dagger (\tilde{b}^\dagger) for nucleons (hyperons), have with spin $i = 0, 1$ (up, down) and isospin $j = 0, 1$ (proton, neutron) indices,

$$\tilde{a}_{i,j}(\vec{n}) = a_{i,j}(\vec{n}) + s_{\text{NL}} \sum_{|\vec{n}'-\vec{n}|=1} a_{i,j}(\vec{n}'), \tag{S5}$$

$$\tilde{b}_i(\vec{n}) = b_i(\vec{n}) + s_{\text{NL}} \sum_{|\vec{n}'-\vec{n}|=1} b_i(\vec{n}'). \quad (\text{S6})$$

In Eq. (S1), V_{Coulomb} represents the Coulomb interaction, and for the details we direct the reader to Ref. [16]. The nonlocal smearing applied on the lattice introduces an explicit dependence on the center-of-mass momentum, thereby breaking Galilean invariance. Consequently, in Eq. (S1) we introduce V_{NN}^{GIR} , $V_{N\Lambda}^{\text{GIR}}$, and $V_{\Lambda\Lambda}^{\text{GIR}}$, which denote the Galilean invariance restoration (GIR) interactions for the nucleon-nucleon, nucleon-hyperon, and hyperon-hyperon interactions, respectively. We refer the reader to Ref. [17] for further details.

Finally, we introduce the three-baryon interactions V_{NNN} , $V_{NN\Lambda}$, and $V_{N\Lambda\Lambda}$, given in Eq. (S1). Recent *ab-initio* nuclear structure and scattering calculations have revealed the significant impact of locally smeared interactions on nuclear binding [18]. Hence, the three-baryon interactions utilized in our calculations are defined with two different choices of local smearing,

$$V_{NNN} = \sum_{i=1,2} \frac{c_{NNN}^{(d_i)}}{6} \sum_{\vec{n}} : \left[\rho^{(d_i)}(\vec{n}) \right]^3 : , \quad (\text{S7})$$

where the parameter d_i denotes the range of local smearing with $0 \leq d_1 < d_2 \leq 3$ (in lattice units). Similarly, the three-baryon interactions consisting of two nucleons and one hyperon are defined with two different choices of local smearing,

$$V_{NN\Lambda} = \sum_{i=1,2} \frac{c_{NN\Lambda}^{(d_i)}}{2} \sum_{\vec{n}} : \left[\rho^{(d_i)}(\vec{n}) \right]^2 \xi^{(d_i)}(\vec{n}) : , \quad (\text{S8})$$

and the interactions involving one nucleon and two hyperons are expressed by also two different choices of local smearing,

$$V_{N\Lambda\Lambda} = \sum_{i=1,2} \frac{c_{N\Lambda\Lambda}^{(d_i)}}{2} \sum_{\vec{n}} : \rho^{(d_i)}(\vec{n}) \left[\xi^{(d_i)}(\vec{n}) \right]^2 : , \quad (\text{S9})$$

where ρ (ξ) is then purely locally smeared nucleon (hyperon) density operator with annihilation and creation operators, a (b) and a^\dagger (b^\dagger) for nucleons (hyperons),

$$\rho^{(d)}(\vec{n}) = \sum_{i,j=0,1} a_{i,j}^\dagger(\vec{n}) a_{i,j}(\vec{n}) + s_{\text{L}}^{3\text{B}} \sum_{|\vec{n}-\vec{n}'|^2=1}^d \sum_{i,j=0,1} a_{i,j}^\dagger(\vec{n}') a_{i,j}(\vec{n}'), \quad (\text{S10})$$

$$\xi^{(d)}(\vec{n}) = \sum_{i=0,1} b_i^\dagger(\vec{n}) b_i(\vec{n}) + s_{\text{L}}^{3\text{B}} \sum_{|\vec{n}-\vec{n}'|^2=1}^d \sum_{i=0,1} b_i^\dagger(\vec{n}') b_i(\vec{n}'). \quad (\text{S11})$$

Here, the parameter d gives the range of local smearing as pointed out above, and $s_{\text{L}}^{3\text{B}}$ defines the strength of the local smearing. In our analysis of locally smeared three-baryon forces given in the above equations, we exclusively consider smearing with ranges $d \leq 3$ in lattice units, corresponding to a physical distance of 1.9 fm. In addition, in Eqs. (S10) and (S11) the local smearing refers to interactions that do not change the positions of particles, while in Eqs. (S5) and (S6) the nonlocal smearing specifies interactions that do change the relative positions of particles. The numerical values of the various LECs and lattice parameters are given below when we discuss nuclei, symmetric nuclear matter as well as hyper-nuclei. We note that throughout we assume that the appearance of the Fermi momentum k_F as a new scale in the problem does not require a re-ordering of the interaction terms, see e.g. Ref. [19].

Auxiliary Field Formulation for Hypernuclear Systems

For a first attempt to investigate ΛN scattering on the lattice, we refer to [20]. The incorporation of the Λ into the nuclear lattice effective field theory framework was considered in Ref. [21] using the impurity lattice Monte Carlo (ILMC) method [22], and this study involved calculating the binding energies of light hypernuclei ${}^3_\Lambda\text{H}$, ${}^4_\Lambda\text{H}$, and ${}^5_\Lambda\text{He}$. The ILMC method treats minority species of fermions, such as hyperons in a nucleus, as worldlines in a medium of majority species of particles simulated by the Auxiliary Field Quantum Monte Carlo (AFQMC) method. Recently, the ILMC method has been extended to enable the study of systems with two impurities [23]. In the present work, we propose a novel approach that allows for the efficient investigation of hypernuclear systems with an arbitrary number of hyperons.

In our lattice simulations, we employ the AFQMC method as it leads to a significant suppression of the sign oscillations. For a comprehensive overview of lattice simulations, the reader is directed to Ref. [2]. AFQMC represents a powerful computational framework within quantum many-body physics, particularly tailored for investigating strongly correlated systems. This method addresses the challenge of solving the full A -body Schrödinger equation by introducing a Hubbard-Stratonovich transformation. This transformation incorporates auxiliary fields to decouple particle densities, thereby enhancing the applicability of Monte Carlo techniques. In essence, within the AFQMC formalism, individual nucleons evolve as if they are single particles in a fluctuating background of auxiliary fields.

The following discussion begins with a discrete auxiliary field formulation for the SU(4) symmetric short ranged two-nucleon interaction given in Eq. (S1),

$$: \exp \left(-\frac{a_t c_{NN}}{2} \tilde{\rho}^2 \right) := \sum_{k=1}^3 w_k : \exp \left(\sqrt{-a_t c_{NN}} s_k \tilde{\rho} \right) : \quad (\text{S12})$$

where a_t is the temporal lattice spacing. From a Taylor expansion of Eq. (S12) we determine the constants s_k and w_k as $s_1 = -s_3 = \sqrt{3}$, $s_2 = 0$, $w_1 = w_3 = 1/6$ and $w_2 = 2/3$.

The nucleon-nucleon interaction given in Eq. (S12) obeys the Wigner SU(4) symmetry [8], which arises from the realization that the combined spin (S) and isospin (T) degrees of freedom of nucleons can be described by a single unified symmetry group. Since we use minimal forces for the hyperon-nucleon and hyperon-hyperon interactions, we now aim to derive an auxiliary field formulation for systems including neutrons, protons and Λ hyperons. This derivation involves replacing the isospin SU $_T$ (2) with flavor SU $_F$ (3) within Wigner's SU(4) symmetry framework, and the combined spin (S) and flavor (F) invariance ultimately leads to the SU(6) symmetry [24]. However, the fact that the strengths of the nucleon-nucleon and hyperon-nuclear interactions are different is breaking this SU(6) symmetry, and there is no longer an approximate symmetry similar to Wigner's SU(4) symmetry used in Eq. (S12). Nevertheless, in the following we exploit the fact that $|c_{NN}| > |c_{N\Lambda}| > |c_{\Lambda\Lambda}|$, which is allowing us to introduce an auxiliary field formulation with an approximate SU(6) symmetry that protects our simulations including Λ hyperons against strong sign oscillations.

The spin and isospin independent two-baryon interactions in Eq. (S1) is expressed as,

$$V_{2B} = \frac{c_{NN}}{2} \sum_{\vec{n}} : [\tilde{\rho}(\vec{n})]^2 : + c_{N\Lambda} \sum_{\vec{n}} : \tilde{\rho}(\vec{n}) \tilde{\xi}(\vec{n}) : + \frac{c_{\Lambda\Lambda}}{2} \sum_{\vec{n}} : [\tilde{\xi}(\vec{n})]^2 : , \quad (\text{S13})$$

and this potential (S13) can be rewritten in the following form,

$$V_{2B} = \frac{c_{NN}}{2} \sum_{\vec{n}} : [\tilde{\phi}(\vec{n})]^2 : + \frac{1}{2} \left(c_{\Lambda\Lambda} - \frac{c_{N\Lambda}^2}{c_{NN}} \right) \sum_{\vec{n}} : [\tilde{\xi}(\vec{n})]^2 : , \quad (\text{S14})$$

where $\tilde{\phi}$ is defined as,

$$\tilde{\phi} = \tilde{\rho} + \frac{c_{N\Lambda}}{c_{NN}} \tilde{\xi} . \quad (\text{S15})$$

In Eq. (S14) the leading contribution comes from the first term in the right-hand side and it is treated non-perturbatively, while the remaining term is computed using first-order perturbation theory. Hence, we define a new Hubbard-Stratonovich transformation for the first term in Eq. (S14), enabling the simulations of systems consisting of both arbitrary number of nucleons and arbitrary number of Λ hyperons with a single auxiliary field,

$$: \exp \left(-\frac{a_t c_{NN}}{2} \tilde{\phi}^2 \right) := \sum_{k=1}^3 w_k : \exp \left(\sqrt{-a_t c_{NN}} s_k \tilde{\phi} \right) : . \quad (\text{S16})$$

It is evident that the solution for the auxiliary field variables s_k and weights w_k is consistent with systems containing only nucleons.

The AFQMC method introduced here broadens hypernuclear calculations by enabling simulations with any number of hyperons. In addition, the approach can be effectively applied to wide range of systems [25, 26]. Let us consider two distinct family of particles and call them A and B , and assume that all interactions are attractive. When the square of the interaction strength between particle types A and B , denoted as c_{AB}^2 , is of comparable magnitude to the product of the interaction strengths within the same particle types, $c_{AA}c_{BB}$, the overall coupling of the second term in Eq. (S14) becomes very small, enabling perturbative treatment and calculations with a single auxiliary field. Furthermore, when $c_{AA}c_{BB} \gg c_{AB}^2$, the second term's overall coupling

is attractive, calculations still can be performed with two auxiliary fields. However, only in the case of $c_{AACBB} \ll c_{AB}^2$, the overall coupling of the second term becomes repulsive which leads to significant sign problems.

Finally, we discuss the two-nucleon interaction $\sim c_{NN}^T$, known to break SU(4) symmetry and to induce significant sign oscillations, which was previously disregarded in minimal nuclear interaction studies [9–14]. In this work, aimed at constraining nuclear forces by using the ground state energies of finite hypernuclei and the saturation properties of symmetric nuclear matter, this isospin interaction is treated non-perturbatively. We employ a Hubbard-Stratonovich transformation and introduce a discrete auxiliary field defined as,

$$: \exp \left(-\frac{a_t c_{NN}^T}{2} \sum_I \tilde{\rho}_I^2 \right) := \sum_{k=1}^3 w_k : \exp \left(\sqrt{-a_t c_{NN}^T} \sum_I s_{k,I} \tilde{\rho}_I \right) : \quad (\text{S17})$$

To minimize the occurring sign oscillations in finite nuclei, we focus on systems with equal numbers of protons and neutrons. Furthermore, in the simulations of pure neutron matter and hyper-neutron matter, this term can be omitted due to the absence of particles breaking isospin symmetry, allowing for sign oscillation-free simulations.

Lattice and computational details

Throughout our calculations presented here, we use a spatial lattice spacing of $a = 1.1$ fm and a temporal lattice spacing of $a_t = 0.2$ fm. We use the local smearing parameter $s_L = 0.06$ and nonlocal smearing parameter $s_{NL} = 0.6$, influencing the strength of locality and nonlocality of the two-baryon interactions, respectively. For the three-baryon interaction, we set the local smearing parameter to $s_L^{3B} = 0.06$. To compute the ground state energies of finite nuclei and hypernuclei, we utilize various periodic cubic lattices ranging in length from 13.2 fm to 19.7 fm. We perform our calculations at different finite Euclidean time steps and extrapolate to the infinite Euclidean time limit using a single and double exponential ansatz [2]. Furthermore, for the computation of pure neutron matter and hyper-neutron matter energies we use lattices with a length of 6.6 fm and impose the average twisted boundary conditions (ATBC) to efficiently eliminate finite volume effects. For further details on ATBC and the extensive analysis demonstrating the negligible impact of finite volume effects when employing ATBC, we refer the reader to Ref. [17].

Symmetric nuclear matter

Before considering the effect of hyperons on the neutron matter EoS, we determine the unknown LECs of the two- and three-nucleon interactions given in Eq. (S1) and predict the EoS corresponding to PNM. For PNM, the neutron-neutron interaction is dominated by the attractive component of the 1S_0 partial wave, and the ($T = 0$) $^3S_1 - ^3D_1$ state does not contribute to the ($T = 1$) neutron-neutron state. The effects of higher partial waves, like P -wave, will be considered in our future work, though the contributions from the P -wave are expected to partially offset each other [27]. In the first step, we pin down the nucleon-nucleon interactions by fitting to the two S -wave phase shifts of nucleon-nucleon scattering as shown in Fig. S1. From these independent scattering phase shift fits we determine the coupling constants as $c_{1S_0} = -1.21 \times 10^{-7} \text{ MeV}^{-2}$ and $c_{3S_1} = -1.92 \times 10^{-7} \text{ MeV}^{-2}$ corresponding with the spin-singlet isospin-triplet and the spin-triplet isospin-singlet channel, respectively, which are related to the LECs given in Eq. (S1) via

$$c_{NN} = (3c_{1S_0} + c_{3S_1})/4, \quad c_{NN}^T = (c_{1S_0} - c_{3S_1})/4. \quad (\text{S18})$$

In the next step, we determine the two LECs of the three-nucleon forces given in Eq. (S7). This is accomplished by obtaining best fits to the saturation properties of symmetric nuclear matter considering all possible combinations of d_1 and d_2 with $0 \leq d_1 < d_2 \leq 3$. Through this process, we arrive at six different sets of interactions, enabling us to quantify the theoretical uncertainty of our calculations. The results for the energy per nucleon in symmetric nuclear matter from the NLEFT calculations are illustrated in Fig. S2. The red shaded area represents the theoretical uncertainty in energies resulting from six different sets of three-nucleon interactions, while the red dashed line denotes the mean value for the energy per nucleon in symmetric nuclear matter, corresponding to the $3N$ interactions with LECs $c_{NNN}^{(1)} = 4.98 \times 10^{-12} \text{ MeV}^{-5}$ and $c_{NNN}^{(3)} = 1.80 \times 10^{-12} \text{ MeV}^{-5}$. The gray shaded area denotes the empirical values. We find the theoretical uncertainty in Fig. S2 is significantly smaller than the empirical uncertainty of the nuclear matter. As a prediction, we find for the compression modulus $K_\infty = 229.0(3.6) \text{ MeV}$, in good agreement with the empirical value of $K_\infty = 240(20) \text{ MeV}$ [29]. The symmetry energy E_{sym} at the saturation density is $35.3 \pm 0.6 \text{ MeV}$, which agree with the ranges of (30–35) MeV based on chiral EFT interactions [30–36], see also the review [37].

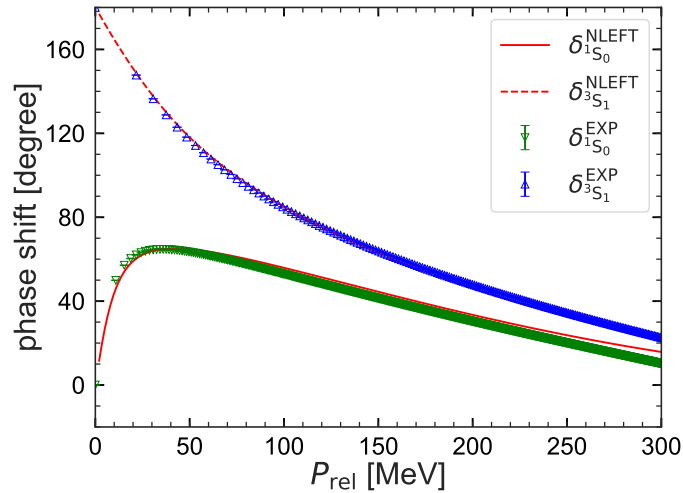


FIG. S1. Plots of the neutron-proton scattering phase shifts as functions of relative momenta. The blue up-triangles and green down-triangles denote the 3S_1 and 1S_0 phase shifts extracted from the Nijmegen partial wave analysis [28], respectively. The solid and dash-dotted curve represents the lattice results for the 1S_0 and the 3S_1 phase shift, in order.

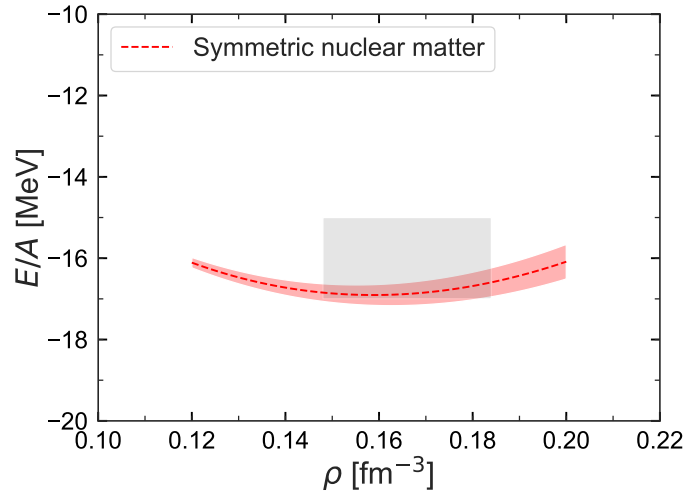


FIG. S2. Energy per nucleon as a function of density for symmetric nuclear matter from the NLEFT calculations. The gray shaded area indicates the empirical values.

Hypernuclei

As it is done in the nucleonic sector, to study the EoS of hyper neutron matter, we first determine the unknown LECs of the interactions involving Λ hyperons. We start again with the two baryon-interactions. For the ΛN interaction, we fit experimental total cross-section data for laboratory momenta below 600 MeV, as shown in the left panel of Fig. S3. Meanwhile, for the $\Lambda\Lambda$ interaction, given the absence of comprehensive cross-section data, we fit to the 1S_0 phase shift derived from chiral EFT at next-to-leading order [38]. From these analyses, we determine the coupling constants as $c_{N\Lambda} = -6.52 \times 10^{-8} \text{ MeV}^{-2}$ and $c_{\Lambda\Lambda} = -2.96 \times 10^{-8} \text{ MeV}^{-2}$.

Similar to our nucleonic studies, we use hypernuclei to constrain the LECs of ΛNN and $\Lambda\Lambda N$ three-baryon forces, more precisely the ground-state energies of single- Λ and double- Λ hypernuclei. A direct comparison of our calculations with experimental results is given for the separation energy, defined as

$$B_{\Lambda}({}^A_{\Lambda}Z) = E({}^{A-1}Z) - E({}^A_{\Lambda}Z), \quad (\text{S19})$$

where E is the energy of the system, A its atomic number and Z its charge. The computation of B thus involves the calculation of the energy of the nucleus ${}^{A-1}Z$ and the corresponding hypernucleus ${}^A_{\Lambda}Z$. In the case of double- Λ hypernuclei, the interesting

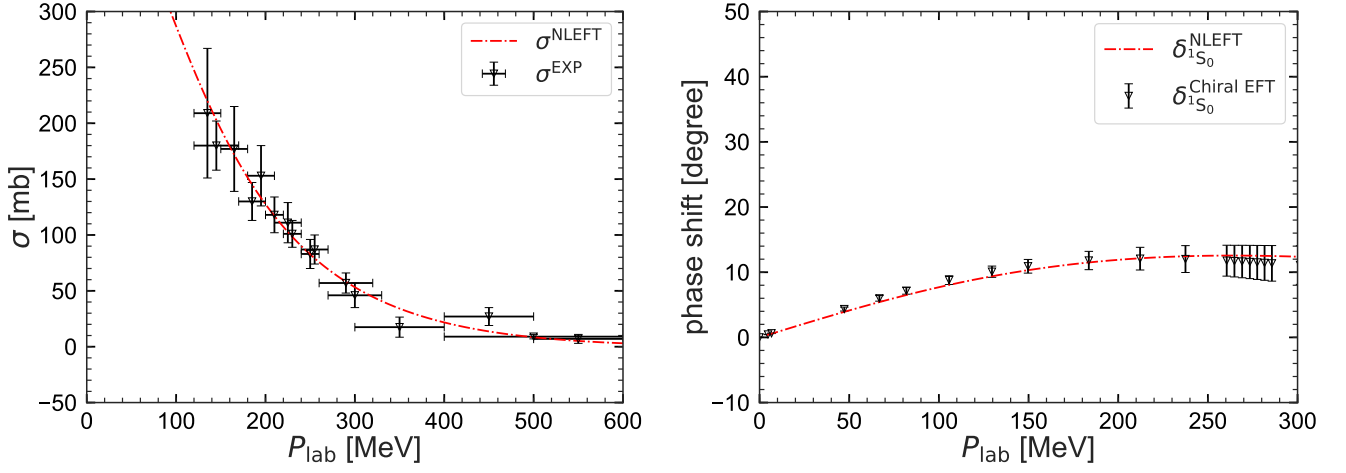


FIG. S3. Baryon-baryon interactions. Left Panel: Fit to the cross section for $N\Lambda$ scattering [39–42]. Right Panel: Fit to the $\Lambda\Lambda$ scattering phase shift from chiral EFT [38].

observable we can access with the NLEFT is the double separation energy,

$$B_{\Lambda\Lambda}(^A_{\Lambda\Lambda}Z) = E(^{A-2}Z) - E(^A_{\Lambda\Lambda}Z). \quad (\text{S20})$$

The calculation of this observable proceeds in the same way in the case single- Λ hypernuclei, starting from the energy of the nucleus, the corresponding Λ hypernucleus and now the double- Λ hypernucleus. The best-fitting results for the separation energies of the various single- Λ and double- Λ hypernuclei, which are used to determine the hyperonic three-body forces given in Eqs.(S8) and (S9), are collected in Tab. S1.

TABLE S1. Λ separation energies for single- Λ and double- Λ hypernuclei (in MeV). The first error is the statistical one whereas the second error is the systematic one (due to the three-baryon forces). The * marks a prediction.

System	NLEFT			Exp.
	HNM(I)	HNM(II)	HNM(III)	
$^5_{\Lambda}\text{He}$	3.40(1)(1)	3.45(1)(2)	3.46(1)(3)	3.10(3)
$^9_{\Lambda}\text{Be}$	5.72(5)(4)	5.64(5)(3)	5.57(5)(3)	6.61(7)
$^{13}_{\Lambda}\text{C}$	10.54(17)(29)*	10.09(17)(27)*	9.80(17)(26)*	11.80(16)
$^6_{\Lambda\Lambda}\text{He}$	6.91(1)(1)	6.91(1)(1)	6.91(1)(1)	6.91(16)

As discussed in the main text, only the separation energies of hypernuclei are utilized to constrain the $N\Lambda$ and $N\Lambda\Lambda$ forces for HNM(I). The hyperonic three-body forces in HNM(II) and HNM(III) are determined by the separation energies of hypernuclei and the Λ threshold densities $\rho_{\Lambda}^{\text{th}}$ around $(2 - 3)\rho_0$. These variations correspond to maximum neutron star masses of $1.59(1)(1) M_{\odot}$, $1.94(1)(1) M_{\odot}$, and $2.17(1)(1) M_{\odot}$, respectively. The HNM(III) approach, which has the largest threshold densities $\rho_{\Lambda}^{\text{th}}$ among the three models, results in the stiffest EoS. This finding underscores the importance of hyperonic three-body forces in achieving higher maximum neutron star masses.

-
- [1] Lee D. Lattice simulations for few- and many-body systems. *Prog Part Nucl Phys* 2009;63:117-154
[2] Lahde TA, Meißner UG. Nuclear lattice effective field theory: an introduction. Heidelberg: Springer 2019;957
[3] Borasoy B, Krebs H, Lee D, et al. The Triton and three-nucleon force in nuclear lattice simulations. *Nucl Phys A* 2006;768:179–193
[4] Lee D, Schafer T. Neutron matter on the lattice with pionless effective field theory. *Phys Rev C* 2005;72:024006
[5] Epelbaum E, Krebs H, Lee D, et al. Ab initio calculation of the hoyle state. *Phys Rev Lett* 2011;106:192501
[6] Elhatisari S, Lee D, Rupak G, et al. Ab initio alpha-alpha scattering. *Nature* 2015;528:111.
[7] Elhatisari S, Bovermann L, Ma YZ, et al. Wavefunction matching for solving quantum many-body problems. *Nature* 2024;630:59-63
[8] Wigner E. On the consequences of the symmetry of the nuclear hamiltonian on the spectroscopy of nuclei. *Phys Rev* 1937;51:106-119
[9] Lu BN, Li N, Elhatisari S, et al. Essential elements for nuclear binding. *Phys Lett B* 2019;797:134863
[10] Lu BN, Li N, Elhatisari S, et al. Ab initio nuclear thermodynamics. *Phys Rev Lett* 2020;125:192502
[11] Ren ZX, Elhatisari S, Lahde TA, et al. Ab initio study of nuclear clustering in hot dilute nuclear matter. *Phys Lett B* 2024;850:138463

- [12] Shen SH, Lähde TA, Lee D, et al. Wigner SU(4) symmetry, clustering, and the spectrum of ^{12}C . *Eur Phys J A* 2021;57:276
- [13] Shen SH, Elhatisari S, Lähde TA, et al. Emergent geometry and duality in the carbon nucleus. *Nature Commun* 2023;14:2777
- [14] Meißner UG, Shen SH, Elhatisari S, et al. Ab initio calculation of the alpha-particle monopole transition form factor. *Phys Rev Lett* 2024;132:062501
- [15] König S, Griebhammer HW, Hammer HW, et al. Nuclear physics around the unitarity limit. *Phys Rev Lett* 2017;118:202501
- [16] Li N, Elhatisari S, Epelbaum E, et al. Neutron-proton scattering with lattice chiral effective field theory at next-to-next-to-next-to-leading order. *Phys Rev C* 2018;98:044002
- [17] Li N, Elhatisari S, Epelbaum E, et al. Galilean invariance restoration on the lattice. *Phys Rev C* 2019;99:064001
- [18] Elhatisari S, Li N, Rokash A, et al. Nuclear binding near a quantum phase transition. *Phys Rev Lett* 2016;117:132501
- [19] Meißner UG, Oller JA, Wirzba A. In-medium chiral perturbation theory beyond the mean field approximation. *Annals Phys* 2002;297:27-66
- [20] Bour S. Hyperon-nucleon interactions on the lattice. Bonn:University of Bonn 2009.
- [21] Frame D, Lähde TA, Lee D, et al. Impurity lattice monte carlo for hypernuclei. *Eur Phys J A* 2020;56:248
- [22] Elhatisari S, Lee D. Fermion-dimer scattering using an impurity lattice monte carlo approach and the adiabatic projection method. *Phys Rev C* 2014;90:064001
- [23] Hildenbrand F, Elhatisari S, Lähde TA, et al. Lattice monte carlo simulations with two impurity worldlines. *Eur Phys J A* 2022;58:167
- [24] Gursev F, Radicati LA. Spin and unitary spin independence of strong interactions. *Phys Rev Lett* 1964;13:173-175
- [25] Sedrakian A, Mur-Petit J, Polls A, et al. Pairing in a two-component ultracold Fermi gas: phases with broken space symmetries. *Phys Rev A* 2005;72:013613
- [26] Zhou L, Cui X, Yi W. Three-component ultracold fermi gases with spin-orbit coupling. *Phys Rev Lett* 2014;112:195301
- [27] Kohno M. Nuclear and neutron matter G-matrix calculations with a chiral effective field theory potential including effects of three-nucleon interactions. *Phys Rev C* 2013;88:064005
- [28] Stoks VGJ, Klomp RAM, Rentmeester MCM, et al. Partial wave analysis of all nucleon-nucleon scattering data below 350-MeV. *Phys Rev C* 1993;48:792-815.
- [29] Garg U, Colò G. The compression-mode giant resonances and nuclear incompressibility. *Prog Part Nucl Phys* 2018;101:55-95
- [30] Hebeler K, Schwenk A. Chiral three-nucleon forces and neutron matter. *Phys Rev C* 2010;82:014314
- [31] Tews I, Krüger T, Hebeler K, et al. Neutron matter at next-to-next-to-next-to-leading order in chiral effective field theory. *Phys Rev Lett* 2013;110:032504
- [32] Holt JW, Kaiser N. Equation of state of nuclear and neutron matter at third-order in perturbation theory from chiral effective field theory. *Phys Rev C* 2017;95:034326
- [33] Drischler C, Hebeler K, Schwenk A. Chiral interactions up to next-to-next-to-next-to-leading order and nuclear saturation. *Phys Rev Lett* 2019;122:042501
- [34] Jiang WG, Ekström A, Forssén C, et al. Accurate bulk properties of nuclei from $A = 2$ to ∞ from potentials with Δ isobars. *Phys Rev C* 2020;102:054301
- [35] Keller J, Hebeler K, Schwenk A. Nuclear equation of state for arbitrary proton fraction and temperature based on chiral effective field theory and a gaussian process emulator. *Phys Rev Lett* 2023;130:072701
- [36] Lim Y, Schwenk A. Symmetry energy and neutron star properties constrained by chiral effective field theory calculations. *Phys Rev C* 2024;109:035801
- [37] Oertel M, Hempel M, Klähn T, et al. Equations of state for supernovae and compact stars. *Rev Mod Phys* 2017;89:015007
- [38] Haidenbauer J, Meißner UG, Petschauer S. Strangeness $S = -2$ baryon-baryon interaction at next-to-leading order in chiral effective field theory. *Nucl Phys A* 2016;954:273-293
- [39] Sechi-Zorn B, Kehoe B, Twitty J, et al. Low-energy lambda-proton elastic scattering. *Phys Rev* 1968;175:1735-1740.
- [40] Alexander G, Karshon U, Shapira A, et al. Study of the lambda-n system in low-energy lambda-p elastic scattering. *Phys Rev* 1968;173:1452-1460.
- [41] Kadyk JA, Alexander G, Chan JH, et al. Lambda p interactions in momentum range 300 to 1500 mev/c. *Nucl Phys B* 1971;27:13-22.
- [42] Hauptman JM, Kadyk JA, Trilling GH. Experimental study of Lambda p and xi0 p interactions in the range 1-GeV/c-10-GeV/c. *Nucl Phys B* 1977;125:29-51.